

Descriptors for Electron and Hole Charge Carriers in Metal Oxides

Daniel W. Davies,^{*,†,||} Christopher N. Savory,^{‡,||} Jarvist M. Frost,[¶] David O. Scanlon,^{‡,||} Benjamin J. Morgan,^{§,||} and Aron Walsh^{*,†,||}

[†]*Department of Materials, Imperial College London, London SW7 2AZ, UK*

[‡]*Department of Chemistry and Thomas Young Centre, University College London, 20 Gordon Street, London WC1H 0AJ, UK*

[¶]*Department of Physics, Imperial College London, London SW7 2AZ, UK*

[§]*Department of Chemistry, University of Bath, Claverton Down, Bath BA2 7AY, UK*

^{||}*The Faraday Institution, Quad One, Harwell Campus, Didcot OX11 0RA, UK*

[⊥]*Diamond Light Source Ltd., Diamond House, Harwell Science and Innovation Campus, Didcot, Oxfordshire OX11 0DE, UK*

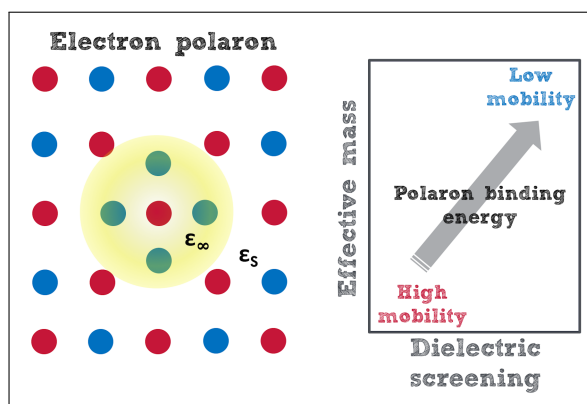
[#]*Department of Materials Science and Engineering, Yonsei University, Seoul 03722, Korea*

E-mail: d.davies16@imperial.ac.uk; a.walsh@imperial.ac.uk

Abstract

Metal oxides can act as insulators, semiconductors or metals depending on their chemical composition and crystal structure. Metal oxide semiconductors, which support equilibrium populations of electron and hole charge carriers, have widespread applications including batteries, solar cells, and display technologies. It is often difficult to predict in advance whether these materials will exhibit localized or delocalized charge carriers upon oxidation or reduction. We combine data from first-principles calculations of the electronic structure and dielectric response of 214 metal oxides to predict the energetic driving force for carrier localization and transport. We assess descriptors based on the carrier effective mass, static polaron binding energy, and Fröhlich electron–phonon coupling. Numerical analysis allows us to assign p and n type transport of a metal oxide to three classes: (i) band transport with high mobility; (ii) small polaron transport with low mobility; and (iii) intermediate behaviour. The results of this classification agree with observations regarding carrier dynamics and lifetimes and are used to predict 10 candidate p-type oxides.

Graphical TOC Entry



Crystalline compounds consisting of metals and oxygen may be electrically insulating (e.g. MgO), semiconducting (e.g. SnO), or even metallic (e.g. TiO).¹ The variation in the behaviour of metal oxides is largely explained by the electronic configuration of the constituent metals. In the case of rocksalt TiO, and assuming formal oxidation states,² Ti(II) is a d^2 cation, which results in a partially occupied t_{2g} d-level in an octahedral crystal field. The crystal structure also plays an important role and it is the edge-sharing network³ of Ti–O octahedra that provides the low energy conduction pathway in the case of TiO.

The mechanisms of electrical conduction in metal oxides with finite band gaps have been the subject of significant research for over a century. Electrolytic conduction can occur from a population of mobile ions, often in the form of charged vacancy or interstitial point defects.⁴ The transport of electron and hole charge carriers is also possible, with some oxides exhibiting high electrical conductivity similar to metals (e.g. In_2O_3 doped n-type with Sn)⁵ and others exhibiting low thermally-activated conductivity similar to disordered semiconductors (e.g. undoped Fe_2O_3).⁶ Metal oxide semiconductors often exhibit a doping asymmetry with a preference for electron or hole conduction,⁷ and the discovery of oxides with robust p-type conductivity remains a major challenge in the field.^{8–10}

In this study, we develop an efficient workflow for assessing the nature of charge carriers in non-metallic crystalline solids. By extracting data from existing metal oxide databases, we first assess the distribution of carrier (electron and hole) effective masses. These are then combined with (high and low-frequency) dielectric tensors to estimate the strength of carrier-lattice coupling in a static polaron model. The resulting binding energies are used to classify metal oxides into three groups. The dynamic electron–phonon interaction for a number of representative compounds are then calculated within Fröhlich electron–phonon coupling theory and an upper limit to the carrier mobility is predicted within the variational Feynman formalism for large (dielectric) polaron transport.

Descriptor 1: Carrier effective mass. The most simple descriptor for conductivity, which has been widely employed in high-throughput searches for p-type and thermoelectric oxides,

is the carrier effective mass, m^* .^{11–15} The effective mass approximation assumes that the response of an electron in a periodic potential is equivalent to that of a free electron with a renormalized mass. There are a number of ways to fit m^* from a band dispersion calculation, $E(k)$.¹⁶ One standard definition is as the local quadratic curvature at the band extrema

$$\frac{1}{m^*} = \frac{1}{\hbar^2} \frac{\partial^2 E}{\partial k^2}. \quad (1)$$

The effective mass describes how easy it is to accelerate the charge carriers. In the Drude model of carrier mobility, electrons with charge e are a classical gas with a constant relaxation time, therefore the mobility is calculated as $\mu = e\tau/m^*$.

This relaxation time τ is the inverse of the sum of all scattering rates (therefore the strongest scattering pathway dominates). Electrical conductivity ($\sigma = \mu n$) additionally depends on the carrier concentration n . Assuming the scattering rate remains constant, a small effective mass ($m^* < 1$) supports a high mobility and conductivity. Asymmetry in the electron and hole effective masses leads to mobility and conductivity differences in n-type ($m_e^* \ll m_h^*$) or p-type ($m_h^* \ll m_e^*$) semiconductors.

The availability of density functional theory (DFT) materials databases including m^* makes it attractive as a low-cost descriptor for high-throughput computational studies. The distribution of electron and hole masses for 5,548 metal oxides calculated by Ricci *et al.*¹⁷ and available from the Materials Project database¹⁸ is shown in Figure 1. The upper valence band of most metal oxides is formed from the weak overlap of relatively localized O 2p orbitals, while the lower conduction band is usually formed of metal s (e.g. ZnO), metal d (e.g. TiO₂) or metal p (e.g. SnO) orbitals with higher principal quantum number. As a result, the hole masses are generally larger and show a wider distribution reflecting the range of crystal environments of oxygen in metal oxide compounds. From the data shown in Figure 1, the electron masses have a mean of 2.5 while the hole masses have a mean of 5.1 m_e . Note the data has been truncated to omit very large values ($m_e > 20$) due to a breakdown in the

effective mass approximation for bands with low dispersion.

The smallest value of electron (hole) effective mass is found for BaSnO₃ (Rb₃AuO), respectively.

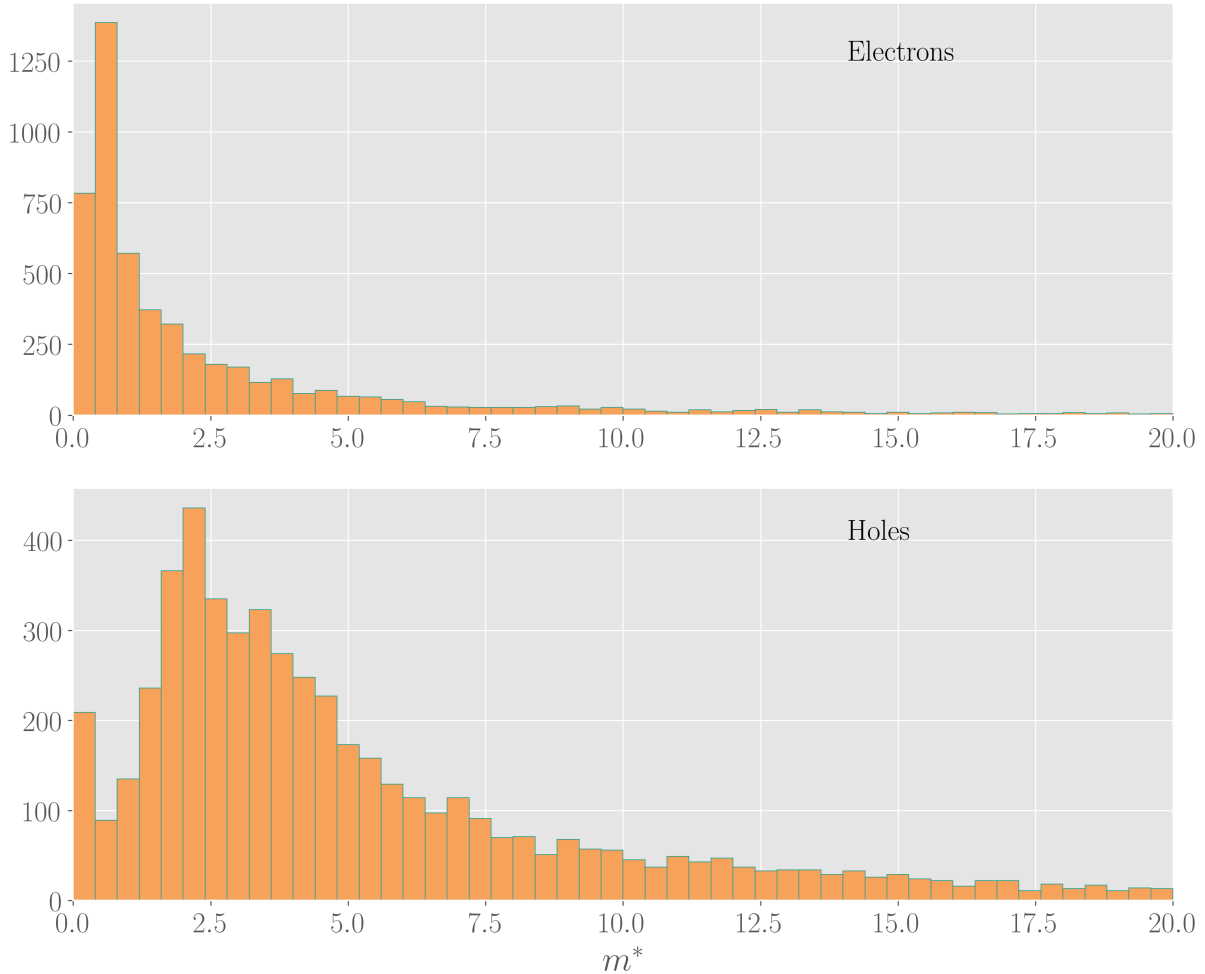


Figure 1: Distribution of electron and hole carrier effective masses (semi-local density functional theory) for 5,548 metal oxides from a public dataset.¹⁷ The values are in units of free electron mass and $m^* < 1$ is typical of conventional band semiconductors, which represents 78% and 11% of the dataset for electrons and holes, respectively.

Descriptor 2: Static polaron binding. Scattering of charge carriers in non-metallic crystals is often dominated by the dielectric polarization of the host.¹⁹ For a static point charge, the long-range polarization is the static (low-frequency) dielectric constant, ϵ_s , which includes both ionic and electronic response. The Pekar factor²⁰ separates out the slow ionic response

(ϵ_{ion}) which can only respond beyond the localised charge carrier, from the fast high-frequency response (ϵ_{∞}) that acts everywhere. The result is an effective dielectric response driving localisation of the charge carrier,

$$\frac{1}{\epsilon_{\text{eff}}} = \left(\frac{1}{\epsilon_{\infty}} - \frac{1}{\epsilon_{\text{s}}} \right). \quad (2)$$

Self-consistently minimizing the total energy of an additional, stationary, effective mass (m^*) charge added to a dielectric crystal with the Pekar dielectric response yields a simple expression for the polaron binding energy of²¹

$$E_{\text{polaron}} = \frac{1}{8\pi^2} \frac{m^* e^4}{\hbar^2 \epsilon_{\text{eff}}^2}. \quad (3)$$

Intuitively, electron localization is favored by large m^* (reduced kinetic energy penalty) and a large difference between ϵ_{∞} and ϵ_{s} (strong dielectric ionic response, and therefore large dielectric electron-phonon coupling). Significant extensions of polaron theory have been since developed to take account of the dynamic properties of both the electron and the lattice including phonon creation and annihilation, as well as other sources of electron-phonon coupling, including the short-range forces that lead to small polaron formation.²²

The availability of datasets for both effective masses¹⁷ and dielectric constants²³ make Eqn. 3 attractive as an alternative descriptor for charge carrier behaviour. It describes the result of the dielectric electron-phonon coupling on a static effective-mass charge carrier. Its coarseness has to be recognised as it assumes isotropic effective masses and dielectric response, and ignores band degeneracy and the angular momentum of the orbitals involved. However, as part of a screening procedure, the $m^*/\epsilon_{\text{eff}}^2$ ratio can differentiate between systems with similar effective masses. The associated energies have been estimated for electrons and holes in each of the 214 metal oxides that are common to both databases.

The distribution of polaron behaviour is shown in Figure 2. The estimated binding energies range from 0.03 meV (an electron in PtO_2) to 1980 meV (a hole in K_3TaO_8). The

general trends follows those of the effective masses and standard expectations, e.g. ZnO with delocalized Zn 4s conduction band has a weak electron binding energy (4 meV), while K_2TiO_3 has a high electron binding energy arising from the localized Ti 3d conduction band (497 meV). In addition to ZnO, other known n-type conductors have weak electron binding energies including SnO_2 and BaSnO_3 (10 and 11 meV, respectively). A number of compounds with similar effective masses are estimated to have very different polaron binding energies. For example, LiRhO_2 and $\text{K}_2\text{SrTa}_2\text{O}_7$ exhibit hole E_{polaron} values of 129 meV and 730 meV, respectively, despite having m_e^* within $0.02 m_e$ of each other.

We can separate the compounds into three types based on the available thermal energy ($k_B T \sim 25 \text{ meV}$) at room temperature: (I) $E_{\text{polaron}} < 25 \text{ meV}$; (II) $25 \text{ meV} < E_{\text{polaron}} < 250 \text{ meV}$; (III) $E_{\text{polaron}} > 250 \text{ meV}$. From the 214 entries, for electrons, there are 66 type I, 141 type II, and 7 type III compounds. For holes, there are 19 type I, 106 type II, and 89 type III compounds. This classification fits with the trends in m^* (Figure 1) and observations that metal oxides are more often n-type (majority electron conductors) than p-type (majority hole conductors).^{24–26} The three types are colored in Figure 2 and a more detailed breakdown is provided in the Supplementary Information.

Descriptor 3: Fröhlich electron–phonon coupling. To assess the limitation of the first two descriptors and to apply these approaches to identify metal oxides with potential for hole delocalization and p-type conduction, we chose a subset of 10 compounds with the smallest $E_{\text{polaron}}^{\text{hole}}$ and performed hybrid-DFT (HSE06)^{27,28} calculations to assess the electronic, vibrational, and dielectric properties. The use of hybrid functionals is necessary to calculate key quantities such as carrier effective masses and Born effective charges accurately, as they both suffer from band gap errors. As a control, we included two materials with large calculated polaron binding energies, namely K_2TiO_3 (electrons) and NaSbO_3 (holes).

Our calculated values for the two descriptors are compared to the public datasets in Table 1 (and Figure S2). The main difference is that the databases used semi-local exchange-correlation functionals (PBE²⁹ for m^* and PBEsol³⁰ for ϵ), which results in a band gap

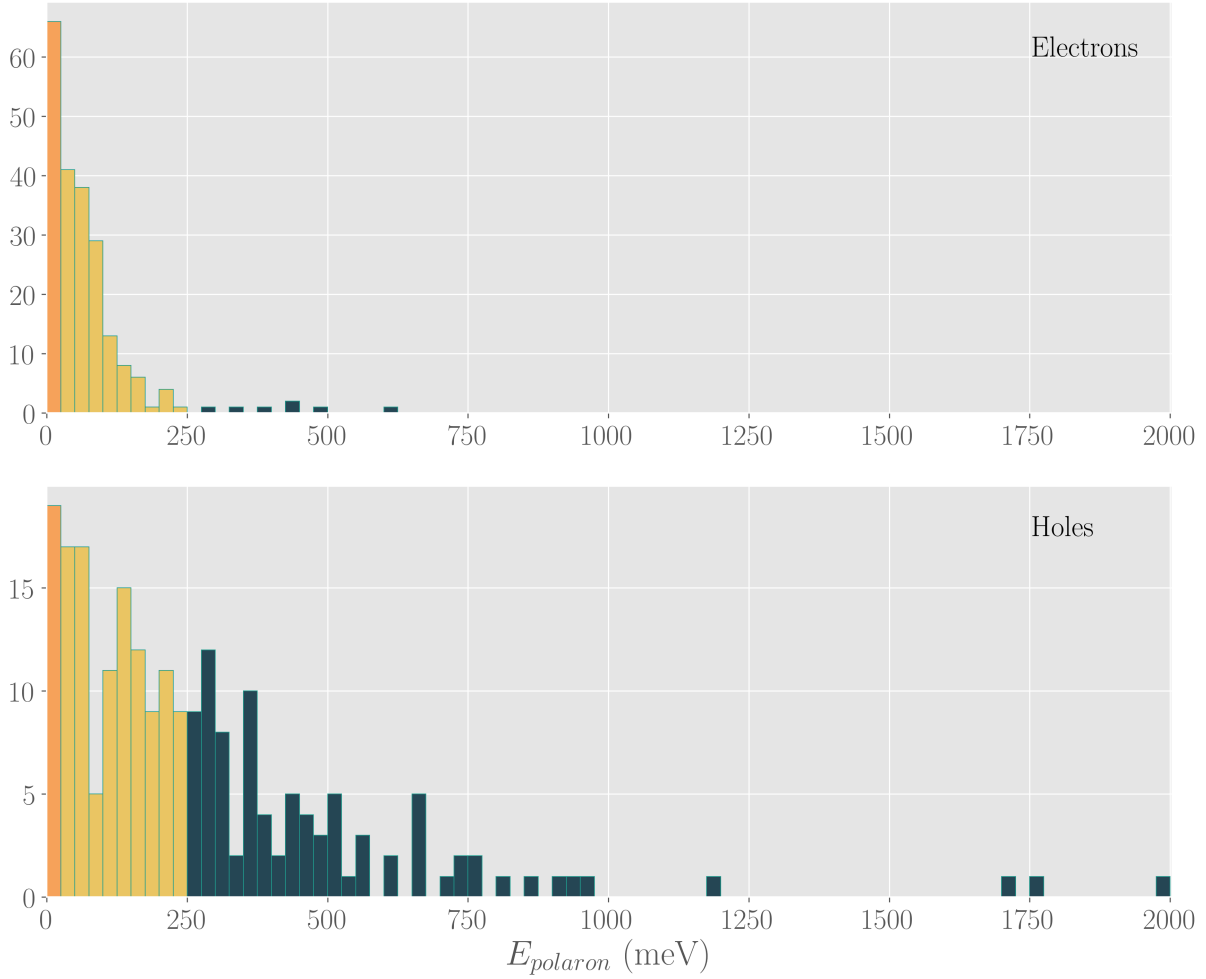


Figure 2: Distribution of electron and hole large polaron binding energies calculated using the effective masses and dielectric constants (semi-local density functional theory)^{17,23} for 214 metal oxides. The values are categorized into type I (orange), II (yellow), and III (blue).

underestimation. For example, the HSE06 band gap of LaZnAsO (1.36 eV) is much closer to the experimentally measured value (1.5 eV)³¹ than the PBE band gap from the database (0.58 eV). In general, from perturbation theory, a smaller band gap is associated with larger estimates of ϵ_∞ (enhanced electronic polarization) and smaller values of m^* (stronger band coupling).³² Hybrid functionals have also been shown directly to improve the description of static and dynamic screening properties compared to semi-local functionals.³³ A particularly bad case is PtO₂, which exhibits the largest discrepancy in ϵ_{eff} . This arises as the dataset value of $\epsilon_\infty = 18.8$ compared to $\epsilon_\infty = 7.1$ from our calculations. Calculations at the Hybrid

DFT level also predict $m_e^* < m_h^*$ for PtO₂ and YZnPO, the opposite trend to that predicted at the GGA level. The qualitative trends are maintained across the series, but the absolute values also show significant variation. This highlights a risk in relying on large materials datasets generated with less computationally expensive methods.

Table 1: Comparison of polaron energies calculated using database values (PBE and PBEsol)^{17,23} and our calculated values (HSE06) for twelve metal oxides. Consideration of the effective optical phonon frequency ω^{optic} (HSE06) also allows the prediction of large polaron mobility (μ) presented at $T = 300$ K. Values are presented as electron / hole.

Formula	E_{polaron} (meV)		ω^{optic} (cm ⁻¹)	μ (cm ² V ⁻¹ s ⁻¹)	m^*	
	database	HSE06			database	HSE06
PtO ₂	0.04 / 0.03	0.52 / 1.48	713	853.4 / 175.1	1.55 / 1.18	0.52 / 1.49
CuRhO ₂	0.14 / 0.54	0.51 / 2.20	590	631.0 / 67.3	0.58 / 2.31	0.50 / 2.18
LiAg ₃ O ₂	3.50 / 2.49	17.51 / 11.35	429	29.7 / 59.9	1.10 / 0.78	0.96 / 0.62
NaNbO ₂	4.86 / 2.64	5.89 / 2.88	464	47.5 / 144.7	1.39 / 0.75	1.27 / 0.62
Ca ₄ Bi ₂ O	3.34 / 4.84	12.46 / 13.68	105	30.6 / 26.2	0.33 / 0.47	0.58 / 0.64
YZnAsO	5.93 / 5.13	17.13 / 29.97	307	28.2 / 11.1	0.47 / 0.41	0.76 / 1.32
NaAg ₃ O ₂	5.21 / 5.99	13.62 / 16.98	439	41.8 / 29.2	1.04 / 1.20	0.83 / 1.03
LaZnAsO	3.19 / 6.02	7.91 / 18.79	281	67.4 / 16.6	0.25 / 0.47	0.48 / 1.14
YZnPO	8.98 / 6.12	13.21 / 18.59	302	45.6 / 26.0	0.85 / 0.58	0.55 / 0.77
LiNbO ₂	24.43 / 6.45	36.28 / 6.62	420	5.6 / 88.4	2.88 / 0.76	3.11 / 0.57
K ₂ TiO ₃	496.6 / 522.8	284.6 / 371.1	370	1.3 / 0.7	2.44 / 2.57	1.70 / 2.22
NaSbO ₃	41.47 / 1182.0	60.67 / 1500	453	32.6 / 0.1	0.41 / 11.7	0.40 / 9.93

Finally, we can directly calculate polaron charge carrier mobility. For polar semiconductors, optic mode (Fröhlich) scattering often limits the relaxation time τ at room temperature and above.³⁴ In addition to the effective mass and dielectric constants, calculation of the carrier mobility also requires knowledge of the optical phonon (ω^{optic}) spectrum and dielectric activity.²¹ These data are used in a calculation of the static dielectric constant, but are often not directly exposed. By computing the phonon modes and energies, along with the Born effective charges, we calculate an effective ω^{optic} following the averaging procedure of Hellwarth.³⁵ The polaron mobility calculation is implemented in the POLARONMOBILITY.JL package,^{36,37} and solves the Feynman variational solution for a finite temperature extension of Fröhlich’s polaron Hamiltonian, and then directly integrates the polaron response function

to produce a mobility. The method is finite temperature, requires no empirical parameters, includes all electron phonon scattering processes. Only considering one scattering process and one source of electron-phonon coupling, the result is always an upper limit to the mobility in a perfect crystal.

The calculated electron and hole mobility values are listed in Table 1. The control K_2TiO_3 was chosen due to its large electron polaron binding energy, and indeed the calculated upper limit to the room temperature mobility of $1 \text{ cm}^2\text{V}^{-2}\text{s}^{-1}$. Similarly, NaSbO_3 which has an even larger hole polaron binding energy has an associated hole mobility of just $0.1 \text{ cm}^2\text{V}^{-2}\text{s}^{-1}$. In terms of the 10 candidate p-type oxides, all have a predicted hole mobility greater than $10 \text{ cm}^2\text{V}^{-2}\text{s}^{-1}$ showing the power of the simpler descriptors. Higher mobilities are predicted for compounds with a higher frequency of ω^{optic} . At $T = 300 \text{ K}$ these have both lower occupancy and are more energetically inaccessible to scatter into, and thus scatter less. For example, the highest hole mobility is predicted for PtO_2 which also has the largest ω^{optic} . Looking in the experimental literature, there is evidence that several of these candidates are indeed p-type semiconductors, including CuRhO_2 ,³⁸ $\text{Li}_{1-x}\text{NbO}_2$,³⁹ and the family of zinc oxyphosphates.^{40,41}

In conclusion, we have considered descriptors for assessing the behaviour of charge carriers in metal oxides, which can be extended to other semiconductors. Our study has shown the utility of modern materials datasets to facilitate rapid screening, but also their limitations both in terms of data quality (level of theory for calculated quantities) and availability (not all values and properties are available, even if they must have been calculated at some point to produce the presented values). Based on the carrier binding energies, we separated the metal oxides into three classes: I (weak coupling) where band transport is expected; II (intermediate behaviour) where the balance between short and long-range forces may be subtle; III (strong coupling) where small polaron transport is expected. One application to identifying p-type metal oxides yielded 10 candidates, which are all predicted to have room temperature hole mobility values greater than $10 \text{ cm}^2\text{V}^{-2}\text{s}^{-1}$.

Going beyond this approach, explicit consideration of defect energies is necessary to predict equilibrium charge carrier concentration and electrical conductivity, but these end up being dependant on the growth environment (chemical potentials) and require the development of appropriate high-throughput procedures and associated databases. Our calculated mobilities represent an upper limit for perfect crystals with no impurity or defect scattering, and with only dielectric electron phonon coupling. The same defect calculations could be used to extend the mobility metric.

Methods and Data Access

Periodic DFT calculations were performed within the Vienna *Ab Initio* Simulation Package (VASP)⁴²⁻⁴⁵ using scalar relativistic pseudopotentials within the projector-augmented wave (PAW) method.⁴⁶ For geometry optimizations, electronic structure and optical property calculations, the functional of Heyd, Scuseria and Ernzerhof (HSE06) was used, with a screening parameter of 0.207 \AA^{-1} .^{27,47} All calculations utilised a plane wave energy cutoff of 600 eV and a consistent \mathbf{k} -point density, with a spacing between \mathbf{k} -points of no more than 0.25 \AA^{-1} , to ensure equivalence between multiple structure types. Convergence criteria of 1×10^{-5} eV and 0.01 eV \AA^{-1} were enforced on the total energy and forces per atom respectively. The high-frequency dielectric function was calculated using the method of Gajdoš *et al.*,⁴⁸ while the ionic response was calculated using Density Functional Perturbation Theory with the related functional of Perdew, Burke and Ernzerhof (PBE).²⁹ The scripts necessary to reproduce the results presented here from raw data, along with the raw data itself, are available from <https://doi.org/10.5281/zenodo.3520679>. This analysis was facilitated by several open-source Python packages, including PYMATGEN,⁴⁹ MATMINER,⁵⁰ SMACT^{51,52} and PHONOPY-SPECTROSCOPY,⁵³ as well as the open-source Julia package POLARONMOBILITY.JL.^{36,37}

Acknowledgement

The research was funded by the Royal Society (grant no. UF130329), the Faraday Institution (grant no. FIRG003), EPSRC (EP/L01551X/1 and EP/N01572X/1) and the European Research Council, ERC, (grant no. 758345). We are grateful to the UK Materials and Molecular Modelling Hub for computational resources, which is partially funded by EPSRC (EP/P020194/1). Via our membership of the UK's HPC Materials Chemistry Consortium, which is funded by EPSRC (EP/L000202, EP/R029431), this work used the ARCHER UK National Supercomputing Service (<http://www.archer.ac.uk>).

Supporting Information Available

The Supporting Information contains data and analysis on trends in polaron binding energies, a summary of the sources of discrepancy between E_{polaron} values calculated using DFT and hybrid-DFT, and a visualization of the variation of ϵ_{eff} with ϵ_s and ϵ_∞ . This material is available free of charge via the Internet at <http://pubs.acs.org/>.

References

- (1) Torrance, J. B.; Lacorre, P.; Asavaroengchai, C.; Metzger, R. M. Why are some oxides metallic, while most are insulating? *Physica C* **1991**, *182*, 351–364.
- (2) Walsh, A.; Sokol, A. A.; Buckeridge, J.; Scanlon, D. O.; Catlow, C. R. A. Oxidation states and ionicity. *Nature Mater.* **2018**, *17*, 958.
- (3) Mizoguchi, H.; Woodward, P. M. Electronic structure studies of main group oxides possessing edge-sharing octahedra: implications for the design of transparent conducting oxides. *Chem. Mater.* **2004**, *16*, 5233–5248.
- (4) Mott, N. F.; Littleton, M. J. Conduction in polar crystals. I. Electrolytic conduction in solid salts. *Trans. Farad. Soc.* **1938**, *34*, 485–499.
- (5) Granqvist, C. G.; Hultåker, A. Transparent and conducting ITO films: new developments and applications. *Thin Solid Films* **2002**, *411*, 1–5.
- (6) Chang, R.; Wagner Jr, J. Direct-current conductivity and iron tracer diffusion in hematite at high temperatures. *J. Am. Ceram. Soc.* **1972**, *55*, 211–213.
- (7) Walsh, A.; Zunger, A. Instilling defect tolerance in new compounds. *Nature Mater.* **2017**, *16*, 964.
- (8) Hautier, G.; Miglio, A.; Ceder, G.; Rignanese, G.-M.; Gonze, X. Identification and design principles of low hole effective mass p-type transparent conducting oxides. *Nature Comm.* **2013**, *4*, 2292.
- (9) Perkins, J. D.; Paudel, T. R.; Zakutayev, A.; Ndione, P. F.; Parilla, P. A.; Young, D.; Lany, S.; Ginley, D. S.; Zunger, A.; Perry, N. H. et al. Inverse design approach to hole doping in ternary oxides: Enhancing p-type conductivity in cobalt oxide spinels. *Phys. Rev. B* **2011**, *84*, 205207.

- (10) Kawazoe, H.; Yanagi, H.; Ueda, K.; Hosono, H. Transparent p-type conducting oxides: design and fabrication of pn heterojunctions. *MRS Bull.* **2000**, *25*, 28–36.
- (11) Hautier, G.; Miglio, A.; Ceder, G.; Rignanese, G.-M.; Gonze, X. Identification and design principles of low hole effective mass p-type transparent conducting oxides. *Nature Communications* **2013**, *4*, 2292.
- (12) Yan, J.; Gorai, P.; Ortiz, B.; Miller, S.; Barnett, S. A.; Mason, T.; Stevanovi, V.; Toberer, E. S. Material descriptors for predicting thermoelectric performance. *Energy Environ. Sci.* **2015**, *8*, 983–994.
- (13) Youn, Y.; Lee, M.; Kim, D.; Jeong, J. K.; Kang, Y.; Han, S. Large-Scale Computational Identification of p-Type Oxide Semiconductors by Hierarchical Screening. *Chemistry of Materials* **2019**, *31*, 5475–5483.
- (14) Chen, W.; Phls, J.-H.; Hautier, G.; Broberg, D.; Bajaj, S.; Aydemir, U.; Gibbs, Z. M.; Zhu, H.; Asta, M.; Snyder, G. J. et al. Understanding thermoelectric properties from high-throughput calculations: trends, insights, and comparisons with experiment. *J. Mater. Chem. C* **2016**, *4*, 4414–4426.
- (15) Kormath Madam Raghupathy, R.; Wiebeler, H.; Khne, T. D.; Felser, C.; Mirhosseini, H. Database screening of ternary chalcogenides for p-type transparent conductors. *Chem. Mater.* **2018**, *30*, 6794–6800.
- (16) Whalley, L. D.; Frost, J. M.; Morgan, B. J.; Walsh, A. Impact of nonparabolic electronic band structure on the optical and transport properties of photovoltaic materials. *Phy. Rev. B* **2019**, *99*, 085207.
- (17) Ricci, F.; Chen, W.; Aydemir, U.; Snyder, G. J.; Rignanese, G.-M.; Jain, A.; Hautier, G. An ab initio electronic transport database for inorganic materials. *Scientific Data* **2017**, *4*, 170085.

- (18) Jain, A.; Ong, S. P.; Hautier, G.; Chen, W.; Richards, W. D.; Dacek, S.; Cholia, S.; Gunter, D.; Skinner, D.; Ceder, G. et al. The Materials Project: A materials genome approach to accelerating materials innovation. *APL Materials* **2013**, *1*, 011002.
- (19) Mott, N. F.; Gurney, R. W. Electronic processes in ionic crystals. **1940**,
- (20) Pekar, S. I. Local quantum states of electrons in an ideal ion crystal. *J. Exp. Theor. Phys.* **1946**, *16*, 341–348.
- (21) Fröhlich, H. Electrons in lattice fields. *Adv. Phys.* **1954**, *3*, 325–361.
- (22) Austin, I.; Mott, N. F. Polarons in crystalline and non-crystalline materials. *Adv. Phys.* **1969**, *18*, 41–102.
- (23) Petretto, G.; Dwaraknath, S.; P.C. Miranda, H.; Winston, D.; Giantomassi, M.; van Setten, M. J.; Gonze, X.; Persson, K. A.; Hautier, G.; Rignanese, G.-M. High-throughput density-functional perturbation theory phonons for inorganic materials. *Scientific Data* **2018**, *5*, 180065.
- (24) Zhang, S.; Wei, S.-H.; Zunger, A. Intrinsic n-type versus p-type doping asymmetry and the defect physics of ZnO. *Phys. Rev. B* **2001**, *63*, 075205.
- (25) Catlow, C. R. A.; Sokol, A. A.; Walsh, A. Microscopic origins of electron and hole stability in ZnO. *Chem. Commun.* **2011**, *47*, 3386–3388.
- (26) Varley, J. B.; Janotti, A.; Franchini, C.; Van de Walle, C. G. Role of self-trapping in luminescence and p-type conductivity of wide-band-gap oxides. *Phys. Rev. B* **2012**, *85*, 081109.
- (27) Heyd, J.; Scuseria, G. E. Efficient hybrid density functional calculations in solids: Assessment of the Heyd–Scuseria–Ernzerhof screened Coulomb hybrid functional. *J. Chem. Phys.* **2004**, *121*, 1187–1192.

- (28) Heyd, J.; Peralta, J. E.; Scuseria, G. E.; Martin, R. L. Energy band gaps and lattice parameters evaluated with the Heyd-Scuseria-Ernzerhof screened hybrid functional. *J. Chem. Phys.* **2005**, *123*, 174101.
- (29) Perdew, J. P.; Burke, K.; Ernzerhof, M. Generalized gradient approximation made simple. *Phys. Rev. Lett.* **1996**, *77*, 3865.
- (30) Perdew, J. P.; Ruzsinszky, A.; Csonka, G. I.; Vydrov, O. A.; Scuseria, G. E.; Constantin, L. A.; Zhou, X.; Burke, K. Restoring the density-gradient expansion for exchange in solids and surfaces. *Phys. Rev. Lett.* **2008**, *100*, 136406.
- (31) Kayanuma, K.; Kawamura, R.; Hiramatsu, H.; Yanagi, H.; Hirano, M.; Kamiya, T.; Hosono, H. Heteroepitaxial growth of layered semiconductors, LaZnOPn ($Pn=\text{P}$ and As). *Thin Solid Films* **2008**, *516*, 5800 – 5804, 5th International Symposium on Transparent Oxide Thin Films for Electronics and Optics.
- (32) Harrison, W. *Elementary Electronic Structure*; World Scientific, 2004.
- (33) Paier, J.; Marsman, M.; Kresse, G. Dielectric properties and excitons for extended systems from hybrid functionals. *Phys. Rev. B* **2008**, *78*, 121201.
- (34) Yu, P. Y.; Cardona, M. *Fundamentals of semiconductors: physics and materials properties*; Springer, 2010.
- (35) Hellwarth, R. W.; Biaggio, I. Mobility of an electron in a multimode polar lattice. *Phys. Rev. B* **1999**, *60*, 299–307.
- (36) Frost, J. M. PolaronMobility.jl: Implementation of the Feynman variational polaron model. *Journal of Open Source Software* **2018**, *3*, 566.
- (37) Frost, J. M. Calculating polaron mobility in halide perovskites. *Phys. Rev. B* **2017**, *96*, 195202.

- (38) Kurita, K.; Sakabayashi, H.; Okazaki, R. Correlation in transport coefficients of hole-doped CuRhO₂ single crystals. *Phys. Rev. B* **2019**, *99*, 115103.
- (39) Rahman, J. U.; Meang, E.-J.; Seo, W.-S.; Hussain, A.; Kim, M. H.; Lee, S. The Synthesis and Thermoelectric Properties of p-Type Li_{1-x}NbO₂-Based Compounds. *J. Elect. Mater.* **2017**, *46*, 1740–1746.
- (40) Kayanuma, K.; Hiramatsu, H.; Hirano, M.; Kawamura, R.; Yanagi, H.; Kamiya, T.; Hosono, H. Apparent bipolarity and Seebeck sign inversion in a layered semiconductor: LaZnOP. *Phys. Rev. B* **2007**, *76*, 195325.
- (41) Kayanuma, K.; Kawamura, R.; Hiramatsu, H.; Yanagi, H.; Hirano, M.; Kamiya, T.; Hosono, H. Heteroepitaxial growth of layered semiconductors, LaZnOP_n (P_n= P and As). *Thin Solid Films* **2008**, *516*, 5800–5804.
- (42) Kresse, G.; Hafner, J. *Ab initio* molecular dynamics for liquid metals. *Phys. Rev. B* **1993**, *47*, 558–561.
- (43) Kresse, G.; Hafner, J. *Ab initio* molecular-dynamics simulation of the liquid-metal amorphous-semiconductor transition in germanium. *Phys. Rev. B* **1994**, *49*, 14251–14269.
- (44) Kresse, G.; Furthmüller, J. Efficient iterative schemes for *ab initio* total-energy calculations using a plane-wave basis set. *Phys. Rev. B* **1996**, *54*, 11169–11186.
- (45) Kresse, G.; Furthmüller, J. Efficiency of *ab initio* total energy calculations for metals and semiconductors using a plane wave basis set. *Comput. Mater. Sci.* **1996**, *6*, 15–50.
- (46) Blochl, P. Projector augmented-wave method. *Phys. Rev. B* **1994**, *50*, 17953–17979.
- (47) Krukau, A. V.; Vydrov, O. A.; Izmaylov, A. F.; Scuseria, G. E. Influence of the exchange screening parameter on the performance of screened hybrid functionals. *J. Chem. Phys.* **2006**, *125*, 224106.

- (48) Gajdoš, M.; Hummer, K.; Kresse, G.; Furthmüller, J.; Bechstedt, F. Linear optical properties in the projector-augmented wave methodology. *Phys. Rev. B* **2006**, *73*, 045112.
- (49) Ong, S. P.; Richards, W. D.; Jain, A.; Hautier, G.; Kocher, M.; Cholia, S.; Gunter, D.; Chevrier, V. L.; Persson, K. A.; Ceder, G. Python Materials Genomics (pymatgen): A robust, open-source python library for materials analysis. *Computational Materials Science* **2013**, *68*, 314–319.
- (50) Ward, L.; Dunn, A.; Faghaninia, A.; Zimmermann, N. E.; Bajaj, S.; Wang, Q.; Montoya, J.; Chen, J.; Bystrom, K.; Dylla, M. et al. Matminer: An open source toolkit for materials data mining. *Computational Materials Science* **2018**, *152*, 60–69.
- (51) Davies, D. W.; Butler, K. T.; Jackson, A. J.; Morris, A.; Frost, J. M.; Skelton, J. M.; Walsh, A. Computational Screening of All Stoichiometric Inorganic Materials. *Chem* **2016**, *1*, 617–627.
- (52) Davies, D. W.; Butler, K. T.; Jackson, A. J.; Skelton, J. M.; Morita, K.; Walsh, A. SMOCT: Semiconducting Materials by Analogy and Chemical Theory. *Journal of Open Source Software* **2019**, *4*, 1361.
- (53) Skelton, J. M.; Burton, L. A.; Jackson, A. J.; Oba, F.; Parker, S. C.; Walsh, A. Lattice dynamics of the tin sulphides SnS₂, SnS and Sn₂S₃: vibrational spectra and thermal transport. *Phys. Chem. Chem. Phys.* **2017**, *19*, 12452–12465.

Descriptors for Electron and Hole Charge Carriers in Metal Oxides

Daniel W. Davies,^{*,†,||} Christopher N. Savory,^{‡,||} Jarvist M. Frost,[¶] David O. Scanlon,^{‡,||} Benjamin J. Morgan,^{§,||} and Aron Walsh^{*,†,||}

[†]*Department of Materials, Imperial College London, London SW7 2AZ, United Kingdom*

[‡]*Department of Chemistry, University College London, 20 Gordon Street, London WC1H 0AJ, United Kingdom*

[¶]*Department of Physics, Imperial College London, London SW7 2AZ, UK*

[§]*Department of Chemistry, University of Bath, Claverton Down, Bath BA2 7AY, United Kingdom*

^{||}*The Faraday Institution, Quad One, Harwell Science and Innovation Campus, Didcot, UK*

[⊥]*Diamond Light Source Ltd., Diamond House, Harwell Science and Innovation Campus, Didcot, Oxfordshire OX11 0DE, United Kingdom*

[#]*Department of Materials Science and Engineering, Yonsei University, Seoul 03722, Korea*

E-mail: d.davies16@imperial.ac.uk; a.walsh@imperial.ac.uk

Supplementary Information

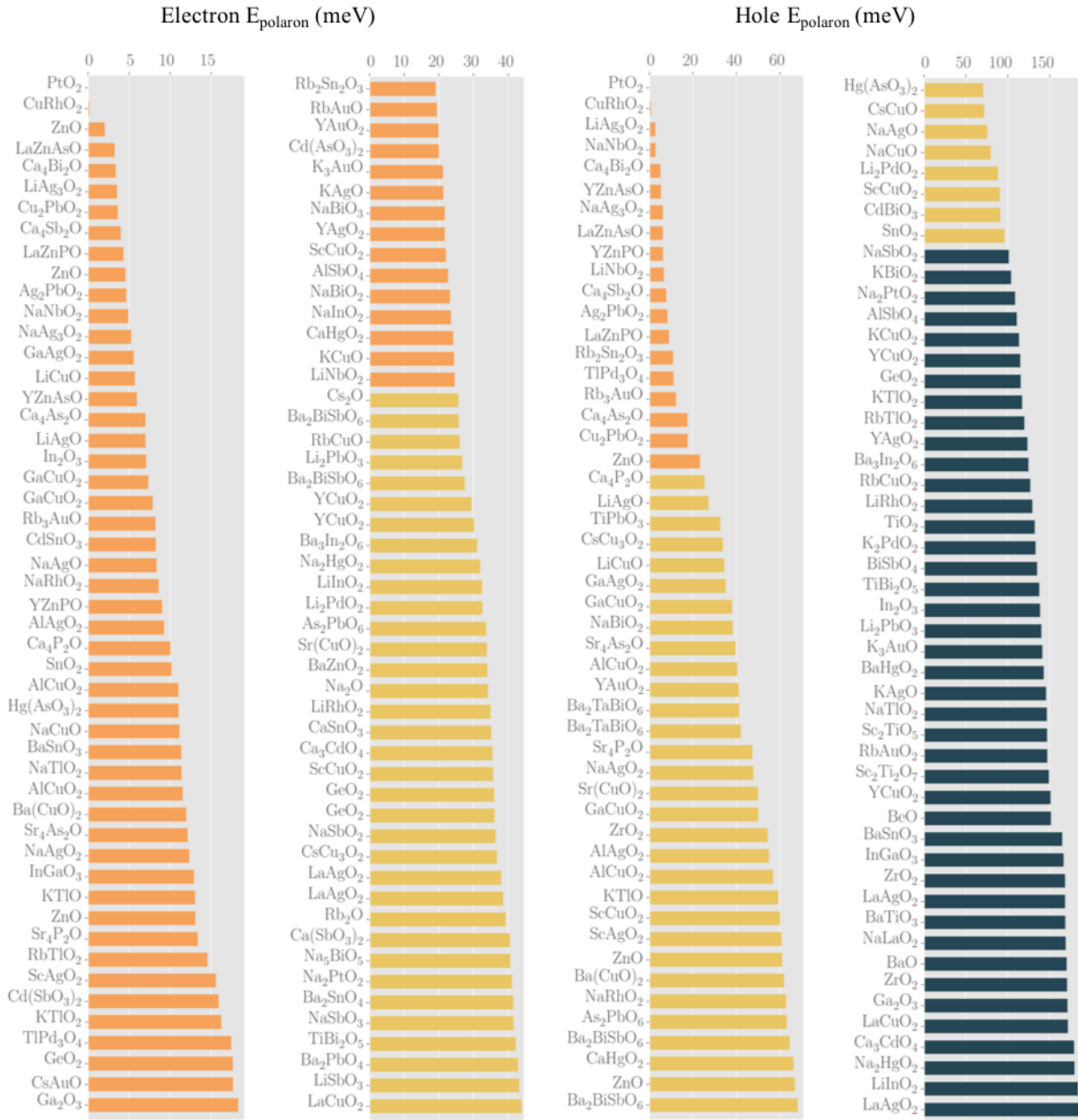


Figure S1: Electron and hole polaron binding energies calculated using the effective masses and dielectric constants from public data-sets. Some compositions have multiple entries due to polymorphism.

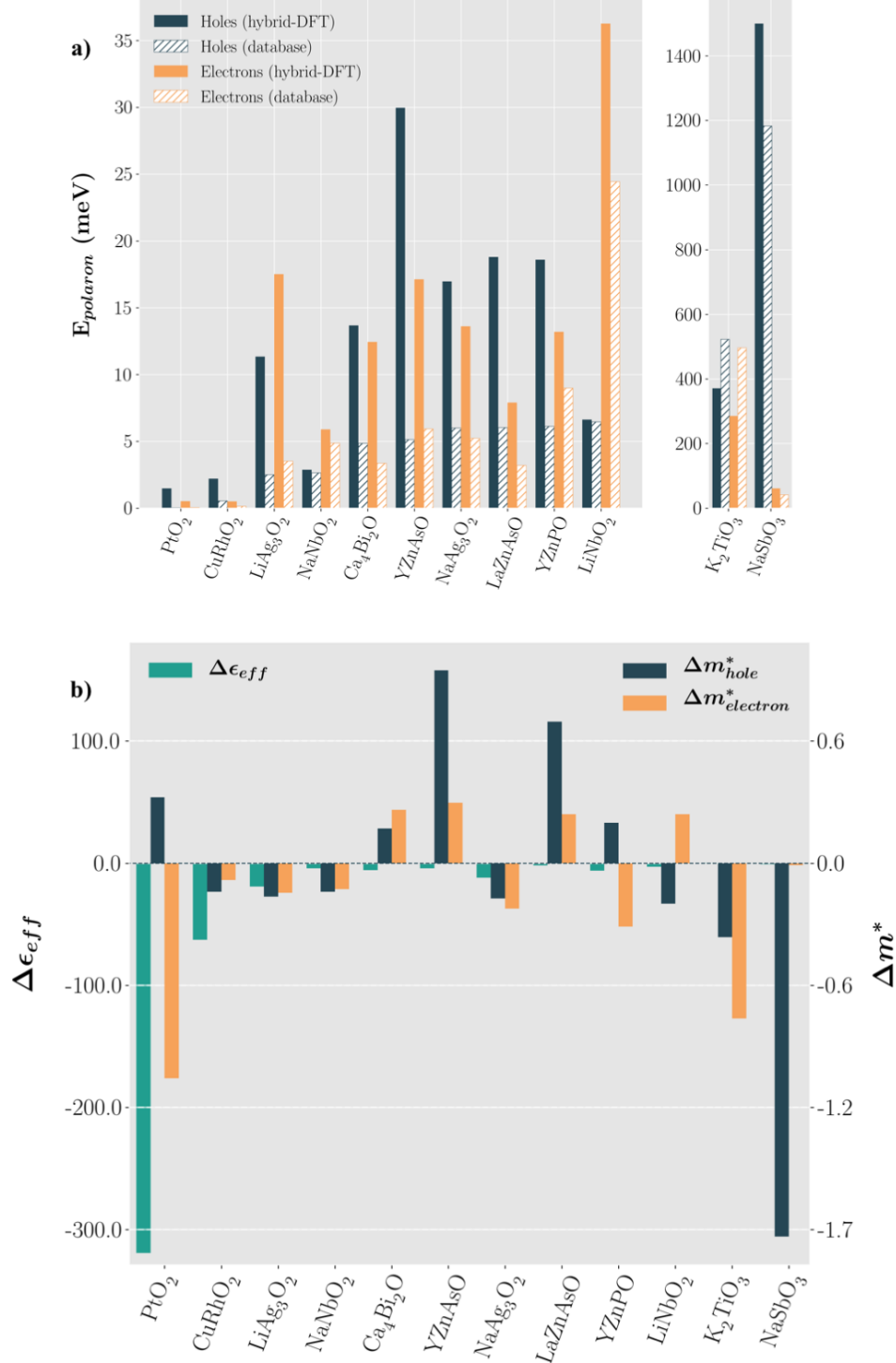


Figure S2: a) Polaron energy ($E_{polaron}$) values as calculated using hybrid-DFT (solid bars) and database (hatched bars) for electrons (orange bars) and holes (blue bars). b) Absolute difference (database derived minus Hybrid-DFT derived) in ϵ_{eff} (green bars) and effective mass (m^*) for electrons (orange bars) and holes (blue bars).

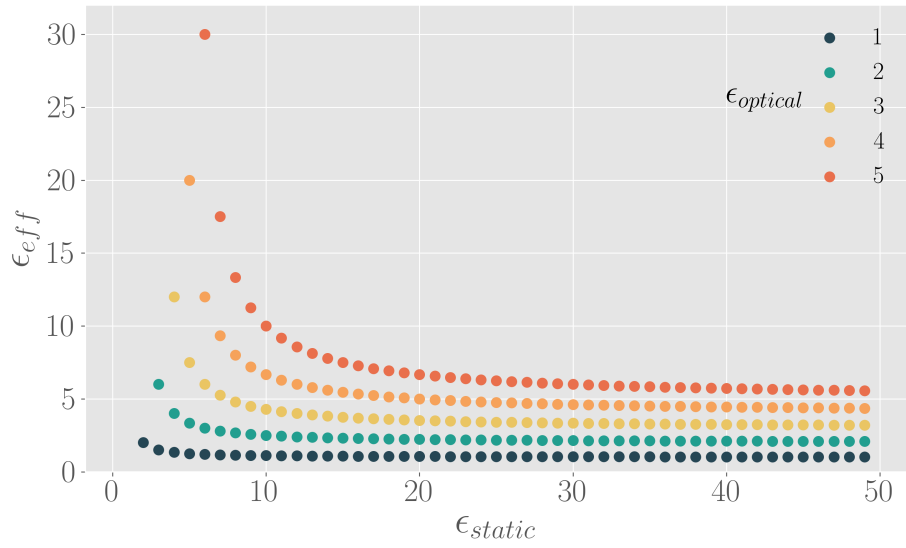


Figure S3: Visualization of the variation of ϵ_{eff} (y-axis) with ϵ_s (x-axis) at different fixed values of ϵ_∞ . For $\epsilon_s > 20$ the system is in a strong screening regime where ϵ_{eff} shows little variation.